analytical chemistry

Article

pubs.acs.org/ac

A Simple Point-of-Care Microfluidic Immunomagnetic Fluorescence Assay for Pathogens

Rui-Qiao Zhang,[†,‡] Shu-Lin Liu,[†] Wei Zhao,[†] Wan-Po Zhang,[§] Xu Yu,[†] Yong Li,[†] An-Jun Li,[†] Dai-Wen Pang,[†,‡] and Zhi-Ling Zhang*[,†,‡]

[†]Key Laboratory of Analytical Chemistry for Biology and Medicine (Ministry of Education), College of Chemistry and Molecular Sciences, State Key Laboratory of Virology, Wuhan University, Wuhan, 430072, People's Republic of China

[‡]Wuhan Institute of Biotechnology, Wuhan, 430075, People's Republic of China

[§]College of Veterinary Medicine, Huazhong Agricultural University, Wuhan, 430070, People's Republic of China

Supporting Information

ABSTRACT: In this work, we reported a simple rapid and point-of-care magnetic immunofluorescence assay for avian influenza virus (AIV) and developed a portable experimental setup equipped with an optical fiber spectrometer and a microfluidic device. We achieved the integration of immunomagnetic target capture, concentration, and fluorescence detection in the microfluidic chip. By optimizing flow rate and incubation time, we could get a limit of detection low up to 3.7×10^4 copy/μL with a sample consumption of 2 μL and a total assay time of less than 55 min. This approach had proved to possess high portability, fast analysis, high specificity, high precision, and reproducibility with an intra-assay variability of 2.87% and an interassay variability of 4.36%. As a whole, this microfluidic system may provide a powerful platform for the rapid detection of AIV and may be extended for detection of other viral pathogens; in addition, this portable experimental setup enables the development of point-of-care diagnostic systems while retaining adequate sensitivity.

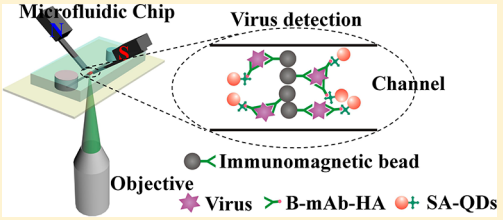

In recent years, infectious diseases, especially emerging or re-emerging infectious agents, such as severe acute respiratory syndrome (SARS), avian influenza, foot-and-mouth disease, dengue disease, and influenza H1N1, have caused devastating effects on social and economic development, threatened human health and life, and become a global health concern. Among them, avian influenza virus (AIV), a lipid enveloped RNA virus that belongs to the *Orthomyxoviridae* family,[1] is an acute viral disease agent of the respiratory tract and causes an abundant economic loss and continues to threaten humans.[2,3] Therefore, the ability of fast, on-site, and sensitive detection for the presence of influenza virus during the early stage of infection is essential to prevent disease spread and provide an immediate and accurate diagnosis. So far, a variety of methods have been used to analyze AIV, such as viral isolation,[4] immunofluorescence (IF) assay,[5,6] enzyme-linked immunosorbent assay (ELISA),[7,8] and real-time polymerase chain reaction (RT-PCR) assay.[9] The acknowledged standard detection method of AIV is virus isolation[3] in cultured cells, eggs, or laboratory animals, followed by the serological methods for final identification.[10] But, it is tedious and time-consuming (1−2 weeks). The molecular diagnostic assays such as PCR and RT-PCR for the detection of influenza infection provide highly sensitive and selective diagnosis protocols. However, these protocols may not be stable with degrading nucleases, nonspecific stains, and cellular debris existing in clinical samples and usually require sophisticated and expensive instrumentation, as well as complicated and multistep sample preparation, which prohibits potential on-site and real-time practical applications. Also, as the well-recognized serological diagnostic method for the detection of influenza infection,[11,12] ELISA is based on the detection of color change or fluorescence labeled on a secondary antibody. A conventional ELISA is usually performed in a 96-well plate and involves a series of tedious processes such as incubation and washing steps. This makes it time-consuming (over 4 h) and labor-intensive requiring well-trained personnel to perform the protocol precisely. In summary, these technologies have played a tremendous effect in clinical diagnosis. However, there are still some shortcomings, such as being time-consuming, processing complexity, low sensitivity, and high cost. Therefore, the development of a rapid, sensitive, point-of-care, and specific method for detecting pathogens is of great importance for preventing and controlling the outbreaks of emerging infectious diseases.

Recently, microfluidic technology and micromachining techniques have enabled miniaturization of biomedical devices and systems, and the microfluidic device has become an attractive tool for biomedical analysis. The integrated microfluidic devices could accomplish the basic stages of biomedical analysis, such as sample preparation, separation and purification, sample transport and mixing, reaction, and detection in a single chip. The unique advantages of the microdevices include rapid analysis,[13] low sample and reagent consumption,[14,15] high

Received: October 5, 2012
Accepted: February 8, 2013
Published: February 8, 2013

integration and versatility in design,[16] portability, and disposability.[17,18] The microfluidic technologies have already been applied in biochemistry, pharmaceutical, clinical diagnosis, and environmental analysis, such as DNA analysis and sequencing,[19,20] immunoassays,[21−23] amino acid and protein analysis,[24,25] cellular assays,[26] bacteria and cell separation,[27−29] virus concentration and purification,[29−33] and single molecules detection.[34] Among the promising applications, immunomagnetic applications have shown considerable potential recently. For instance, our previous study[23] has shown that immunomagnetic beads functionalized with rabbit antigoat IgG could be directly immobilized in the microchannel through the plus electromagnetic field, and then, a magnetic reaction area can be formed to capture goat IgG. Chen et al.[30] used magnetic nanoparticle conjugated antibody to concentrate and purify HIV particles from human plasma samples, which were captured in a magnetic bed for the subsequent lysis and analysis. They demonstrated that an 80-fold concentration for 1 mL of initial sample and a 44-fold concentration for 0.5 mL of initial sample could be obtained.

Many efforts have been devoted to the development of immunoassay based on superparamagnetic bead which have the unique advantages such as high surface-to-volume ratio providing more conjugating sites, easy functionalizing with biochemical agents, and easy handling by using magnets or magnetic coils.[35−37] For clinical samples, separation and recognition of targets are essential steps for precise detection, and functional magnetic beads can be for this usage. Indeed, magnetic beads conjugated with functional groups have been successfully applied in microfluidic systems for immunoassays,[23,38,39] mRNA isolation,[40] virus RNA detection,[41] dynamic DNA hybridization,[42] protein digestion,[43] biomedical diagnosis,[44,45] and cell sorting.[46,47] The application of functional magnetic beads in the microfluidic system enhanced the target specific separation.[48]

In this study, a microfluidic immunomagnetic fluorescence assay for AIV was proposed, incorporated with immunomagnetic beads forming a magnetic reaction area for AIV concentration and high-luminance quantum dots (QDs) conjugated with streptavidin (QDs-SA) to quantify H9N2 virus through fluorescence intensity. For fluorescence detection, we assembled three experimental setups (Figure 3). The third experimental setup based on an optical fiber spectrometer (Figure 3-3) was portable and suitable for point-of-care. We mainly used the first two methods to verify the feasibility that the portable optical fiber spectrometer could carry out fluorescence detection. The entire detection assay process including incubation and detection steps could be completed within less than 55 min, and the limit of detection was 3.7×10^4 copy/μL. As a whole, this microfluidic system may provide a powerful platform for the rapid detection of AIV and may be extended for detection of other types of viruses with high specificity and sensitivity; in addition, this portable experimental setup enables the development of point-of-care diagnostic systems while retaining adequate sensitivity.

EXPERIMENTAL SECTION

Reagents and Materials. AZ50XT photoresist (PR) was obtained from AZ Electronic Materials (AZ Electronic Materials Corp., USA). Superparamagnetic beads (MasterBeads Carboxylic Acid 0215, 500 nm diameter) were obtained from AdemTech (Pessac, France). Polydimethylsiloxane (PDMS) and curing agent were purchased from GE (GE Toshiba Silicones Co., Ltd., Japan). *N*-Ethyl-*N*′-(3-dimethyl-aminopropyl)-carbodiimide hydrochloride (EDAC) and *N*-hydroxysuccinimide (NHS) were purchased from Sigma. Bovine serum albumin (BSA) was obtained from Biosharp. A Qdots 605 streptavidin conjugate (SA-QDs) was purchased from Wuhan Jiayuan Quantum Dots Co., Ltd. Mouse monoclonal antibody to AIV H9N2 hemagglutinin (mAb-HA) was purchased from Sino Biological Inc. The mAb-HA was biotinylated (B-mAb-HA) with an EZ-link sulfo-NHS-LC-biotinylation kit purchased from Pierce Biotechnology (Rockford, IL). Ultrapure water (18.2 MΩ·cm) supplied by a Millipore water-purification system (Synergy UV, Millipore, USA) was used to prepare buffer solutions. The inactivated AIV H9N2, the inactivated AIV H5N1, the inactivated AIV H1N1, infectious bursal disease virus (IBDV), and egg drop syndrome (EDS) were obtained from Wuhan Institute of Virology, Chinese Academy of Sciences.

Microfluidic Chip Design and Fabrication. The microfluidic device was fabricated by soft lithography and rapid prototyped with PDMS technology.[49] The AZ50XT PR was spin-coated onto a clean, smooth silicon wafer at 1200 rpm for 30 s to obtain a 30 μm thick film. This wafer was baked at 75 °C for 4 min and 105 °C for 8 min on a contact hot plate. Then, it was cooled and exposed with a mask (12 000 dpi, Shanghai Kaisheng Electronic CO., Ltd., China) under UV light; the PR was developed in an AZ 400 K developer (1:2.5 v/v AZ400k/H_2O) for 3 min. Then, the wafer was washed with water and dried with N_2 gas. The AZ50XT master pattern on a silicon wafer was fabricated. Before PDMS casting, the master was treated with trimethylchlorosilane vapor for 3 min to prevent the adhesion between PDMS and the silicon wafer.

For the PDMS replica molding, first, two handmade miniature bars guiding magnetism were placed on the position beside the central channel with an angle of 120°, and the angle between the plane of the two miniature bars and that of the microfluidic channel was fixed at 90°, and then, PDMS A and B components were mixed at a ratio of 10:1 and casted on the AZ50XT master pattern. After baking at 75 °C for 3 h, the PDMS molding was peeled off from the master carefully after cooling to room temperature and punched with a blunt needle for inlets and outlets. Finally, the PDMS mold and a glass slide were treated by oxygen plasma, irreversible bonded, and baked at 75 °C for 10 min. The layout and the photograph of the microfluidic device were showed in Figure 1a and c. The

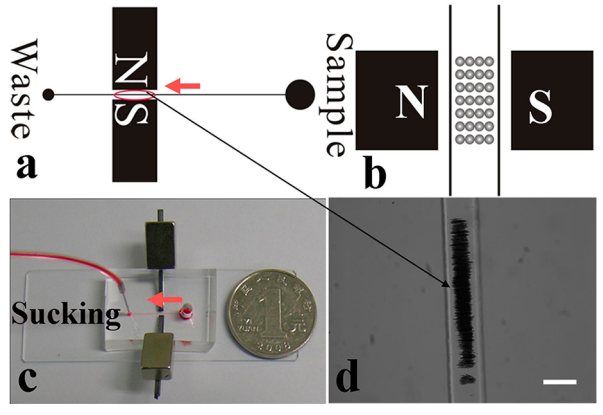

Figure 1. (a) Layout and (c) photograph of an integrated microfluidic device. (b) Schematic diagram and (d) photograph of magnetic trapping, oriented by 90°. The scale bar is 100 μm.

microchannel was 100 μm wide and 30 μm high. The superparamagnetic beads coated with mAb-HA, 0.01 mol/L phosphate-buffered saline (PBS, pH = 7.4), H9N2 virus, B-mAb-HA, and SA-QDs were sucked into the microchannel by the way of pump pulling in order.

Generating the Magnetic Reaction Area. An amount of 1 μL of superparamagnetic beads, suspended in 200 μL of 0.01 mol/L PBS (pH 7.4), was sonicated for 1 min to reduce aggregation. A 0.5 μL amount of this solution was then sucked into the microchannel at a flow rate of 30 μL/h with a multisyringe pump (TS2-60, Baoding Longer Precision Pump Co., Ltd. China). At the magnetic zone, the superparamagnetic beads self-organized in columns parallel to the magnetic field. With the bead accumulation, a stable magnetic reaction area (Figure 1d) was formed in the channel of the magnetic zone.

Preparation of Immunomagnetic Beads with mAb-HA. EDAC and NHS were used to activate the carboxyl groups on the superparamagnetic beads (500 nm diameter), according to the protocol as in our previous report.[23] The activated magnetic beads were covalently coupled to mAb-HA to form mAb-HA coated magnetic beads (immunomagnetic beads), and the final product was stored in 0.01 mol/L pH 7.4 PBS with 1% BSA, 0.1% Tween, and 0.02% sodium azide at 4 °C. The conjugation process and characterization of the immunomagnetic beads were described in detail in the Supporting Information, S.2.

Procedure for Microfluidic Immunomagnetic Fluorescence Assay of AIV H9N2. AIV H9N2 detection was based on the sandwich immunomagnetic fluorescence assay. All the solutions were prepared in 0.01 mol/L PBS (pH 7.4). The solutions were sucked into the microchannel at a flow rate of 30 μL/h. Magnetic beads coated with mAb-HA were sucked into the microchannel (Figure 2a) and captured in the magnetic zone to form the magnetic reaction area (Figure 2b). Then, H9N2 virus and B-mAb-HA were sequentially sucked into the microchannel and incubated (Figure 2c–f). Finally the SA-QDs solution (a dilution of 1:100, nearly 10 nmol/L) was sucked into the microchannel (Figure 2g) and incubated (Figure 2h). After washing with PBS, the fluorescence signal was detected at the magnetic reaction zone. After detection, removing the external magnetic field, magnetic beads with all reagents were flushed out (Figure 2i), and the microchip was ready for another immunoassay. Between each two steps, the microchannel was washed with PBS.

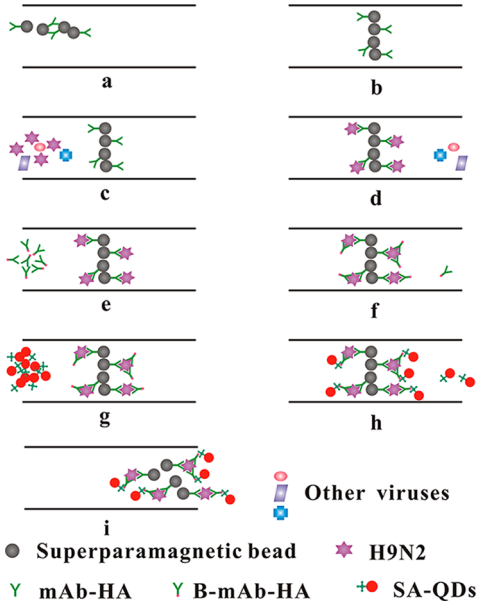

Figure 2. Schematic representation of the experiment protocol for magnetic immunoassay. (a) Suction of superparamagnetic beads into the microchannel; (b) capturing superparamagnetic beads with the magnetic field; (c) sucking H9N2; (d) incubating; (e) sucking B-mAb-HA; (f) incubating; (g) sucking SA-QDs; (h) incubating; (i) flushing everything out.

Fluorescence Detection of the Magnetic Reaction Area. For fluorescence detection, we assembled three experimental setups (Figure 3, the photographs of the three experimental setups were shown in Figure S3 of the Supporting Information). For the first method (Figure 3-1), the chip was horizontally mounted on the stage of an inverted fluorescence microscope (Olympus IX70) for visualization. Images were acquired using a high-sensitivity digital camera (E5400, Nikon). Brightfield images were obtained under the microscope-mounted halogen lamps. For fluorescence images, a Hg lamp (USH-1030L) source was used in conjunction with a fluorescence microscopy filter cube (Omega optical). The light passed through an excitation filter (band pass 510–550 nm) and was reflected from a dichroic mirror (DM: near unity reflectivity below 570 nm and near-unity transmissivity above 590 nm) to excite QDs in the magnetic reaction area of the microchip through the microscope objective. The fluorescence signal from the sample was transmitted down through the microscope objective, dichroic mirror, and the barrier filter (long pass near-unity transmissivity above 590 nm) to the camera, and then, the fluorescence images were acquired.

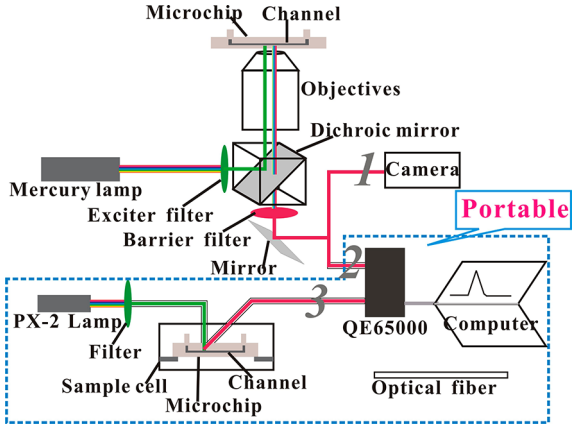

Figure 3. Schematic diagram of the integration fluorescence detection setups.

For the second method (Figure 3-2), the experimental setup was roughly the same to the first method, only with the camera replaced by the portable optical fiber spectrometer (QE65000, Ocean Optics), and then, the fluorescence signal was exported with the form of the spectrum on the computer.

For the third method (Figure 3-3), the experimental setup was built by ourselves. The entire device was extremely portable and suitable for on-site testing. The chip was mounted horizontally in a sample cell (a homemade dark-chamber). A pulsed xenon light source (PX-2 lamp) sent light through a filter via an input fiber into the dark-chamber in a chamber holder to excite QDs in the magnetic reaction area of the microchip (the input fiber was vertical to the microchip). Then,

dx.doi.org/10.1021/ac302903p | Anal. Chem. 2013, 85, 2645–2651

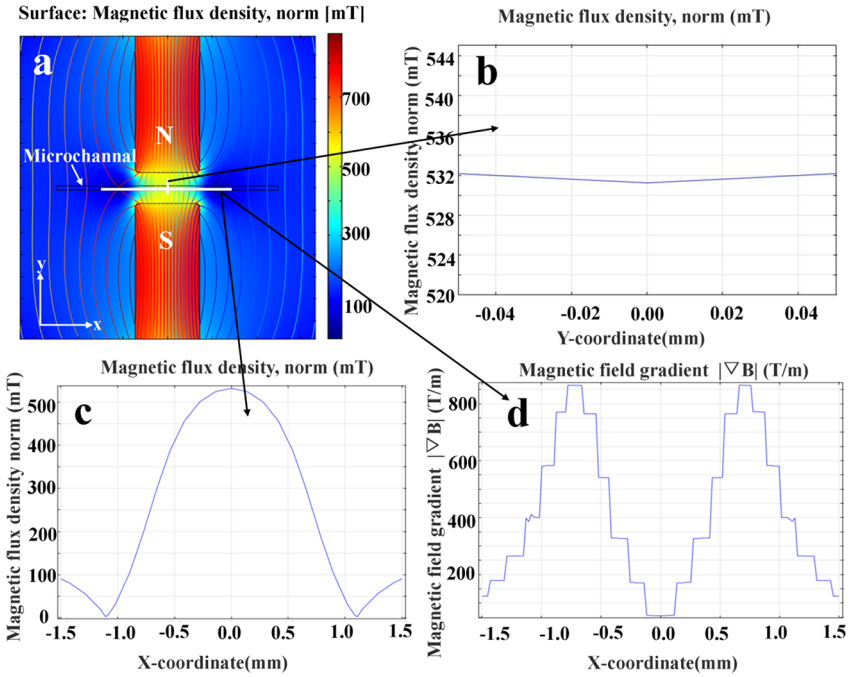

Figure 4. (a) Simulation of the induced magnetic field distribution produced by the two magnets. (b) Variation of the magnetic flux density along the Y axis in the region of 100 μm (width of microchannel). (c) Variation of the magnetic flux density along the X axis in the region of 3 mm. (d) Variation of the magnetic field gradient along the X axis in the region of 3 mm.

the fluorescence light (605 ± 5 nm) was transmitted through the output fiber to the spectrometer connected to the computer. When the input fiber and the output fiber were at a 45° angle to each other, the light through the input fiber and the output fiber intersected at the magnetic reaction area of the microchip, and low scattering background and high signal-to-noise ratio were realized.[50]

In this paper, we mainly used the first two methods to verify the feasibility that the portable optical fiber spectrometer could carry out fluorescence detection. Fluorescence images of the magnetic reaction zone were acquired using an Olympus inverted fluorescence microscope equipped with a high-sensitivity digital camera. Fluorescence intensity detection of the magnetic reaction zone was based on a portable optical fiber spectrometer. In the same way, background noise was measured from the outside of the magnetic reaction zone in the channel.

Numerical Simulation of the Magnetic Field. The magnetic field could be described as the magnetic flux density (B) or the magnetic field intensity (H). In this work, we placed two handmade miniature bars guiding magnetism beside the central channel with a slope angle of 120°, which used to guide magnetism of two permanent magnets into the central channel to generate the magnetic field (as shown in Figure 1c), so the magnetic part is static. The constitutive equation describes the relation between B and H:

$$B = \mu_0 \mu_r H + B_r \quad (1)$$

where μ_0 is the permeability of a vacuum ($4\pi \times 10^{-7}$, H/m), μ_r is the relative permeability of the magnets, H is the magnetic field intensity (A/m), and B_r is the remanent magnetic flux density, which is the magnetic flux density where no magnetic field was present. COMSOL Multiphysics 4.2a software was used to simulate the magnetic flux density distribution.

RESULTS AND DISCUSSION

Numerical Simulation of the Magnetic Field. The chip model was shown in Figure 4a. We regarded the two bars guiding magnetism as two magnets. The microchannel (100 μm width) was put in the middle of the two magnets with a distance of 600 μm. Two magnets (length × width × height = 4 mm × 1.46 mm × 1.18 mm) were arranged with opposite poles (NS poles). We assumed the relative permeability of the magnets (μ_r) was 1.05 and the remanent magnetic flux density of the permanent magnets (B_r) was measured to be about 1 T. We used 2D COMSOL multiphysics/electromagnetics/magnetostatics to simulate the magnetic field distribution in the microchannel. Figure 4a was the simulation of the induced magnetic field distribution produced by the two magnets. Figure 4b was the variation (about 0.94 mT) of the magnetic flux density on the 100 μm length scale along the Y axis direction. The width of our chips was 100 μm, so we could regarded the magnetic field distribution as uniform along the Y axis direction in our chip. From the results (Figure 4c), the variation of the magnetic flux density was about 530 mT in the microchannel along the X axis direction in the region of 3 mm. The stable magnetic reaction area (Figure 1d) was about 500 μm length, and the magnetic flux density of the stable magnetic reaction area was over 530 mT. The variations of the magnetic field gradient were about from 50 to 860 T/m along the X axis in the region of 3 mm (Figure 4d).

Generated the Stable Magnetic Reaction Area. In microfluidic chips, the magnetic beads would experience the Stokes drag force. The hydrodynamic drag force on a magnetic bead can be evaluated by the Stokes' equation:[51,52]

$$F_d = 6\pi\eta r\Delta v \quad (2)$$

where η is the viscosity of the fluid (kg/(m·s)), r is the radius of the magnetic bead (m), and Δv is the difference in velocity of the magnetic bead and the medium surrounding the magnetic

dx.doi.org/10.1021/ac302903p | Anal. Chem. 2013, 85, 2645−2651

bead (m/s). We sucked magnetic beads into the microchannel at a flow velocity of 30 μL/h; thus, the typical hydrodynamic drag force acting on a magnetic bead was below 13 pN.

When a strong magnetic field (B) is applied via external permanent magnets, the magnetic force exerted on the bead is taken as[53]

$$F_m = \frac{4}{3}\pi\rho r^3 M\nabla B \quad (3)$$

where r is the radius, ρ is the density of the bead, M is the saturation magnetization (~40 (A·m^2)/kg), and ∇B (Supporting Information, S.1) is the magnetic field gradient (T/m). The magnetic field gradient in the local areas on the Y axis increased greatly (from 50 to 860 T/m) in our device. The magnetic force (from 1.8 to 20 pN) acting on a magnetic bead was sufficient to exceed the hydrodynamic drag force under the operating conditions. Therefore, the magnetic beads could be captured and form the stable magnetic reaction area as in our design.

Optimization of the Microfluidic Immunomagnetic Fluorescence Assay Conditions. *Optimization of Flow Rate.* When optimizing the flow rate, the incubation time was set as 5 min, and the different flow rates were set as 10, 20, 30, 40, and 50 μL/h. Finally, we got the best flow rate through comparing the fluorescence intensity of the magnetic reaction area at 605 nm. The fluorescence intensity first decreased very slowly with the increasing flow rate and then decreased remarkably after 30 μL/h (as shown in Figure 5). Such a phenomenon indicated that the flow rate was lower and the fluorescence intensity was higher, but considering the time-consuming nature of the whole experimental process, we set 30 μL/h as the optimum flow rate.

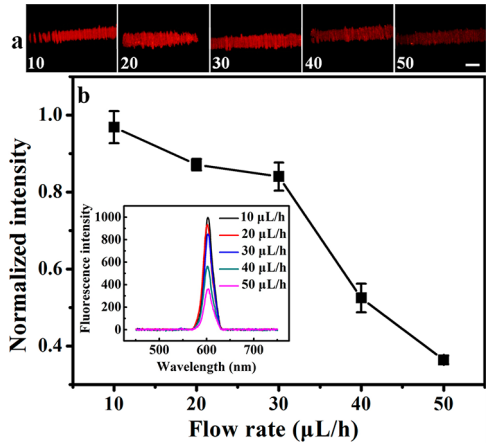

Figure 5. (a) Fluorescence images resulting from the immunoassay with 3.0 × 10^7 copy/μL H9N2 of the different flow rates. (b) Calibration fluorescence intensity curve of the different flow rates. Error bars = ± standard deviation (SD), and n = 3. The corresponding fluorescence spectra were shown in the insert. The scale bar is 50 μm.

Optimization of Incubation Time. Then, under the optimized flow rate of 30 μL/h, three periods of incubation time for magnetic beads to H9N2 (Figure 2d), H9N2 to B-mAb-HA (Figure 2f), and B-mAb-HA to SA-QDs (Figure 2h) were optimized by orthorhombic analysis. The fluorescence intensity of the magnetic reaction area at 605 nm was set as the index. The SAS software 9.1 was used to analyze the experimental results. The details of the experimental design and result analysis were described in the Supporting Information, S.4. From the analysis results, the optimal conditions of incubation time were as follows: 15.4, 16.2, and 11.1 min in order. Considering the time-consuming nature of the whole experimental process, we set the three optimum incubation time as 15, 15 min and 10 min in order, and the entire assay procedure including sample incubation and virus detection took less than 55 min.

Quantitative Assay of Microfluidic Immunomagnetic Fluorescence Detection. Quantitative immunoassay detection was carried out under optimum conditions as described above. Fluorescence images resulting from the sandwich immunoassay of H9N2 virus with concentrations varying from 3.0 × 10^5 to 1.2 × 10^8 copy/μL were shown in Figure 6a. The corresponding fluorescence spectra, displaying the same trends with the fluorescence images were shown in Figure 6b. The calibration curve of the fluorescence intensity versus the H9N2 virus concentration was shown in Figure 6c. It could be seen that the fluorescence intensity increased linearly in the range from 3.0 × 10^5 to 1.2 × 10^7 copy/μL (Figure 6c, insert). Further increasing the H9N2 virus concentration resulted in a plateau in the fluorescence intensity, which indicated that H9N2 virus captured in the magnetic reaction area was saturated with a concentration of 6.0 × 10^7 copy/μL. The limit of detection (LOD) was 3.7 × 10^4 copy/μL (LOD = 3SD/slope, n = 9). For these assays, the amount of reagent consumed was low, which reduced the cost per assay. Therefore, the integrated microfluidic device was promising for further applications in bioanalysis fields. The total assay time was less than 55 min in the whole process including all incubation and detection steps.

Specificity of Microfluidic Immunomagnetic Fluorescence Assay. To test the specificity of this method, we detected the reagents blank including the H9N2 control, the B-mAb-HA control, and the both control by using PBS buffer to replace H9N2 and/or B-mAb-HA, several common avian viruses such as inactive H5N1, H1N1, EDS, and IBDV as negative controls, and 6.0 × 10^6 copy/μL H9N2 as the positive sample. The results showed that this method owned perfect specificity. Typical fluorescence spectra were shown in Figure 7b. The QDs emission peak was easily detected in the positive sample, while no obvious QDs peaks were found in the three blanks. The negative samples had very low QDs peaks, but their fluorescence intensity was below the LOD.

Precision and Reproducibility of Microfluidic Immunomagnetic Fluorescence Assay. To further evaluate the applicability of this detection method at the point-of-care, we used the intra-assay and interassay variabilities to present the precision and reproducibility of the microfluidic immunomagnetic fluorescence test results. The intra-assay variability was the variability of the same sample analyzed in parallel several times, and the 6.0 × 10^6 copy/μL H9N2 sample was detected five times with the same batch of immunomagnetic beads to test the intra-assay variability. The interassay variability was tested in the same way but using five different batches of immunomagnetic beads for detecting 6.0 × 10^6 copy/μL H9N2 samples. The intra-assay and interassay variabilities were calculated by the coefficient of variability (CV% = SD/mean) of the parallel results. The values of 2.87% and 4.36% for intra- and interassay, respectively, (Table 1) proved the well precision and the well reproducibility of this detection method.

Complex biological samples including fresh dung, liver, and lung were used to investigate reliability of this method. The

dx.doi.org/10.1021/ac302903p | Anal. Chem. 2013, 85, 2645−2651

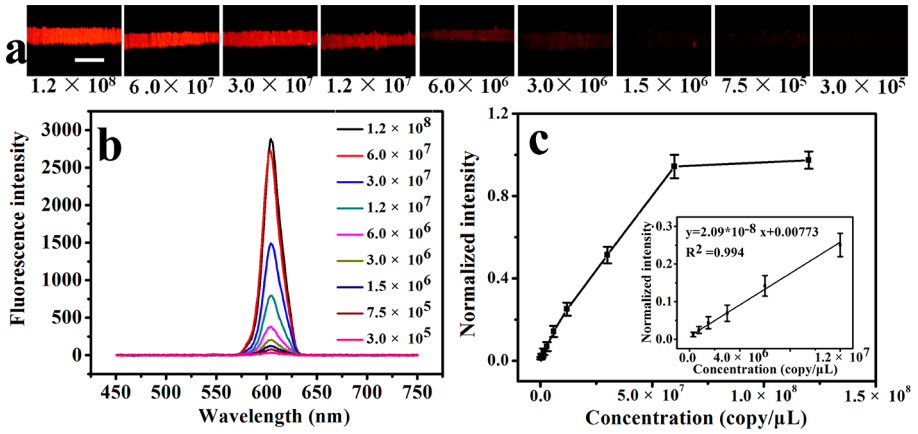

Figure 6. (a) Fluorescence images resulting from the immunoassay with H9N2 concentrations varying from 3.0×10^5 to 1.2×10^8 copy/μL. (b) Corresponding fluorescence spectra, displaying the same trends with the fluorescence images. (c) Calibration curve of the fluorescence intensity versus the H9N2 virus concentration and (insert) the linear relationship of fluorescence intensity versus H9N2 virus concentration from 3.0×10^5 to 1.2×10^7 copy/μL. Error bars = ±SD, and n = 3. The scale bar is 100 μm.

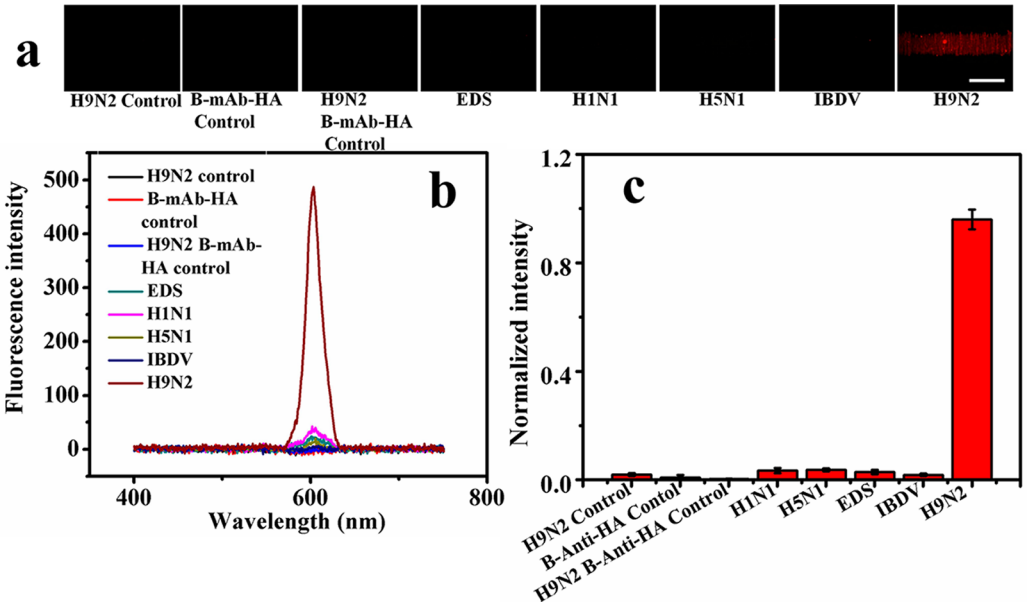

Figure 7. (a) Fluorescence images for the results of the specificity of this method with the reagents blank including H9N2, B-mAb-HA, and both, several common avian viruses inactive H5N1, H1N1, EDS, and IBDV as negative samples, and a positive sample of H9N2. (b) Corresponding fluorescence spectra, displaying the same trends with the fluorescence images. (c) Histogram for the results of the specificity of this method. Error bars = ±SD, and n = 3. The scale bar is 100 μm.

Table 1. Intra- and Interassay Variability of This Method

	mean	SD	CV (%) n = 5
intra-assay	495.99	14.26	2.87
interassay	511.48	22.32	4.36

experimental details and analysis of results were described in the Supporting Information, S.5. All positive samples with different tissues and dung presented the obvious QDs signals, while signals of negative samples were all below the LOD. The results suggested that this method could be applied to detect virus in the complex biological samples.

CONCLUSION

We have proposed a rapid simple and highly sensitive immunomagnetic fluorescence detection approach of virus based on an integrated microfluidic device. The experiment has been performed successfully and showed the expected feasibility. The total assay time of this method was less than 55 min in the whole process. The detection limit was 3.7×10^4 copy/μL, and the sample consumption was low, only 2 μL. The specificity of this method by detecting the reagents blank and several other avian viruses has validated perfect. Also, it was proved that the method could be used to detect virus in complex samples. The rapid, sensitive, point-of-care method for detecting pathogens and the fluorescence sandwich immunoassay principle can be expanded to detect other pathogens.

ASSOCIATED CONTENT

Supporting Information

Additional information as noted in the text. This material is available free of charge via the Internet at http://pubs.acs.org.

dx.doi.org/10.1021/ac302903p | Anal. Chem. 2013, 85, 2645−2651

AUTHOR INFORMATION

Corresponding Author

*Phone: 0086-27-68756759; fax: 0086-27-68754067; e-mail: zlzhang@whu.edu.cn.

Notes

The authors declare no competing financial interest.

ACKNOWLEDGMENTS

This work was supported by the National Basic Research Program of China (973 Program, 2011CB933600), the Science Fund for Creative Research Groups of NSFC (20921062), the National Natural Science Foundation of China (20875072, 21175100), the Program for New Century Excellent Talents in University (NCET-10-0656), and the "3551 Talent Program" of the Administrative Committee of East Lake Hi-Tech Development Zone (Grant [2011]137).

REFERENCES

(1) Sidorenko, Y.; Reichl, U. *Biotechnol. Bioeng.* **2004**, *88*, 1−14.
(2) Peiris, J. S. M.; de Jong, M. D.; Guan, Y. *Clin. Microbiol. Rev.* **2007**, *20*, 243−267.
(3) Subbarao, K.; Katz, J. *Cell. Mol. Life Sci.* **2000**, *57*, 1770−1784.
(4) Swayne, D. E.; Avellaneda, G.; Mickle, T. R.; Pritchard, N.; Cruz, J.; Bublot, M. *Avian Dis.* **2007**, *51*, 697−704.
(5) Shibata, T.; Tanaka, T.; Shimizu, K.; Hayakawa, S.; Kuroda, K. *J. Virol. Methods* **2009**, *156*, 162−165.
(6) Zhao, W.; Zhang, W. P.; Zhang, Z. L.; He, R. L.; Lin, Y.; Xie, M.; Wang, H. Z.; Pang, D. W. *Anal. Chem.* **2012**, *84*, 2358−2365.
(7) Sala, G.; Cordioli, P.; Moreno-Martin, A.; Tollis, M.; Brocchi, E.; Piccirillo, A.; Lavazza, A. *Avian Dis.* **2003**, *47*, 1057−1059.
(8) Chua, T. H.; Ellis, T. M.; Wong, C. W.; Guan, Y.; Ge, S. X.; Peng, G.; Lamichhane, C.; Maliadis, C.; Tan, S. W.; Selleck, P.; Parkinson, J. *Avian Dis.* **2007**, *51*, 96−105.
(9) Boivin, G.; Côté, S.; Déry, P.; De Serres, G.; Bergeron, M. G. *J. Clin. Microbiol.* **2004**, *42*, 45−51.
(10) Charlton, B.; Crossley, B.; Hietala, S. *Comp. Immunol. Microbiol. Infect. Dis.* **2009**, *32*, 341−350.
(11) Chomel, J. J.; Thouvenot, D.; Onno, M.; Kaiser, C.; Gourreau, J. M.; Aymard, M. *J. Virol. Methods* **1989**, *25*, 81−91.
(12) Zhang, A. D.; Jin, M. L.; Liu, F. F.; Guo, X. B.; Hu, Q. Y.; Han, L.; Tan, Y. D.; Chen, H. C. *Avian Dis.* **2006**, *50*, 325−330.
(13) Chen, D. F.; Mauk, M.; Qiu, X. B.; Liu, C. C.; Kim, J. T.; Ramprasad, S.; Ongagna, S.; Abrams, W. R.; Malamud, D.; Corstjens, P. L.; Bau, H. H. *Biomed. Microdevices* **2010**, *12*, 705−719.
(14) Kim, S. J.; Shin, G. W.; Choi, S. J.; Hwang, H. S.; Jung, G. Y.; Seo, T. S. *Electrophoresis* **2010**, *31*, 1108−1115.
(15) Dittrich, P. S.; Tachikawa, K.; Manz, A. *Anal. Chem.* **2006**, *78*, 3887−3907.
(16) Hagan, K. A.; Reedy, C. R.; Uchimoto, M. L.; Basu, D.; Engel, D. A.; Landers, J. P. *Lab Chip* **2011**, *11*, 957−961.
(17) Liu, P.; Seo, T. S.; Beyor, N.; Shin, K. J.; Scherer, J. R.; Mathies, R. A. *Anal. Chem.* **2007**, *79*, 1881−1889.
(18) Tanaka, Y.; Sato, K.; Shimizu, T.; Yamato, M.; Okano, T.; Kitamori, T. *Lab Chip* **2007**, *7*, 207−212.
(19) Chou, C. F.; Bakajin, O.; Turner, S. W. P.; Duke, T. A. J.; Chan, S. S.; Cox, E. C.; Craighead, H. G.; Austin, R. H. *Proc. Natl. Acad. Sci. U.S.A.* **1999**, *96*, 13762−13765.
(20) Goedecke, N.; McKenna, B.; El-Difrawy, S.; Carey, L.; Matsudaira, P.; Ehrlich, D. *Electrophoresis* **2004**, *25*, 1678−1686.
(21) Horsman, K. M.; Bienvenue, J. M.; Blasier, K. R.; Landers, J. P. *J. Forensic Sci.* **2007**, *52*, 784−799.
(22) Kim, Y. T.; Chen, Y. C.; Choi, J. Y.; Kim, W. J.; Dae, H. M.; Jung, J.; Seo, T. S. *Biosens. Bioelectron.* **2012**, *33*, 88−94.
(23) Liu, Y. J.; Guo, S. S.; Zhang, Z. L.; Huang, W. H.; Baigl, D.; Chen, Y.; Pang, D. W. *J. Appl. Phys.* **2007**, *102*, 084911−084916.
(24) Connatser, R. M.; Cochran, M.; Harrison, R. J.; Sepaniak, M. J. *Electrophoresis* **2008**, *29*, 1441−1450.
(25) Peterson, D. S.; Rohr, T.; Svec, F.; Fréchet, J. M. J. *Anal. Chem.* **2002**, *74*, 4081−4088.
(26) McClain, M. A.; Culbertson, C. T.; Jacobson, S. C.; Allbritton, N. L.; Sims, C. E.; Ramsey, J. M. *Anal. Chem.* **2003**, *75*, 5646−5655.
(27) Sethu, P.; Moldawer, L. L.; Mindrinos, M. N.; Scumpia, P. O.; Tannahill, C. L.; Wilhelmy, J.; Efron, P. A.; Brownstein, B. H.; Tompkins, R. G.; Toner, M. *Anal. Chem.* **2006**, *78*, 5453−5461.
(28) Cheng, X. H.; Gupta, A.; Chen, C. C.; Tompkins, R. G.; Rodriguez, W.; Toner, M. *Lab Chip* **2009**, *9*, 1357−1364.
(29) Balasubramanian, A. K.; Soni, K. A.; Beskok, A.; Pillai, S. D. *Lab Chip* **2007**, *7*, 1315−1321.
(30) Chen, G. D.; Alberts, C. J.; Rodriguez, W.; Toner, M. *Anal. Chem.* **2010**, *82*, 723−728.
(31) Akin, D.; Li, H. B.; Bashir, R. *Nano Lett.* **2004**, *4*, 257−259.
(32) Connelly, J. T.; Kondapalli, S.; Skoupi, M.; Parker, J. S. L.; Kirby, B. J.; Baeumner, A. J. *Anal. Bioanal. Chem.* **2012**, *402*, 315−323.
(33) Lien, K. Y.; Lin, J. L.; Liu, C. Y.; Lei, H. Y.; Lee, G. B. *Lab Chip* **2007**, *7*, 868−875.
(34) Shen, Z.; Liu, X. J.; Long, Z. C.; Liu, D. Y.; Ye, N. N.; Qin, J. H.; Dai, Z. P.; Lin, B. C. *Electrophoresis* **2006**, *27*, 1084−1092.
(35) Kuramitz, H. *Anal. Bioanal. Chem.* **2009**, *394*, 61−69.
(36) Moros, M.; Pelaz, B.; López-Larrubia, P.; García-Martin, M. L.; Grazú, V.; de la Fuente, J. M. *Nanoscale* **2010**, *2*, 1746−1755.
(37) Child, H. W.; del Pino, P. A.; De la Fuente, J. M.; Hursthouse, A. S.; Stirling, D.; Mullen, M.; McPhee, G. M.; Nixon, C.; Jayawarna, V.; Berry, C. C. *ACS Nano* **2011**, *5*, 7910−7919.
(38) Yang, S. Y.; Lien, K. Y.; Huang, K. J.; Lei, H. Y.; Lee, G. B. *Biosens. Bioelectron.* **2008**, *24*, 855−862.
(39) Hayes, M. A.; Polson, N. A.; Phayre, A. N.; Garcia, A. A. *Anal. Chem.* **2001**, *73*, 5896−5902.
(40) Jiang, G. F.; Harrison, D. J. *Analyst* **2000**, *125*, 2176−2179.
(41) Zaytseva, N. V.; Montagna, R. A.; Baeumner, A. J. *Anal. Chem.* **2005**, *77*, 7520−7527.
(42) Fan, Z. H.; Mangru, S.; Granzow, R.; Heaney, P.; Ho, W.; Dong, Q. P.; Kumar, R. *Anal. Chem.* **1999**, *71*, 4851−4859.
(43) Slovakova, M.; Minc, N.; Bilkova, Z.; Smadja, C.; Faigle, W.; Fütterer, C.; Taverna, M.; Viovy, J. L. *Lab Chip* **2005**, *5*, 935−942.
(44) Kartalov, E. P.; Zhong, J. F.; Scherer, A.; Quake, S. R.; Taylor, C. R.; Anderson, W. F. *BioTechniques* **2006**, *40*, 85−90.
(45) Lien, K. Y.; Lee, W. C.; Lei, H. Y.; Lee, G. B. *Biosens. Bioelectron.* **2007**, *22*, 1739−1748.
(46) Furdui, V. I.; Harrison, D. J. *Lab Chip* **2004**, *4*, 614−618.
(47) Furdui, V. I.; Kariuki, J. K.; Harrison, D. J. *J. Micromech. Microeng.* **2003**, *13*, S164−S170.
(48) Gijs, M. A. M. *Microfluid. Nanofluid.* **2004**, *1*, 22−40.
(49) Duffy, D. C.; McDonald, J. C.; Schueller, O. J. A.; Whitesides, G. M. *Anal. Chem.* **1998**, *70*, 4974−4984.
(50) Fu, J. L.; Fang, Q.; Zhang, T.; Jin, X. H.; Fang, Z. L. *Anal. Chem.* **2006**, *78*, 3827−3834.
(51) Pankhurst, Q. A.; Connolly, J.; Jones, S. K.; Dobson, J. *J. Phys. D: Appl. Phys.* **2003**, *36*, R167−R181.
(52) Yu, X.; Feng, X.; Hu, J.; Zhang, Z. L.; Pang, D. W. *Langmuir* **2011**, *27*, 5147−5156.
(53) Ferguson, B. S.; Buchsbaum, S. F.; Wu, T. T.; Hsieh, K.; Xiao, Y.; Sun, R.; Soh, H. T. *J. Am. Chem. Soc.* **2011**, *133*, 9129−9135.